◆ Human Brain Mapping 38:974–986 (2017) ◆

In-Vivo Measurements of Human Brain Tissue Conductivity Using Focal Electrical Current Injection Through Intracerebral Multicontact Electrodes

Laurent Koessler,[1,2,3]* Sophie Colnat-Coulbois,[4] Thierry Cecchin,[1,2] Janis Hofmanis,[5] Jacek P. Dmochowski,[6] Anthony M. Norcia,[7] and Louis G. Maillard[1,2,3]

[1]*CNRS, CRAN, UMR 7039, Vandœuvre-lès-Nancy, France*
[2]*Université de Lorraine, CRAN, UMR 7039, Vandœuvre-lès-Nancy, 54516, France*
[3]*Service de Neurologie, Centre Hospitalier Universitaire de Nancy, Nancy, 54000, France*
[4]*Service de Neurochirurgie, Centre Hospitalier Universitaire de Nancy, Nancy, 54000, France*
[5]*Ventspils Engineering Research Institute, Ventspils University, Ventspils, LV3601, Latvia*
[6]*Department of Biomedical Engineering, City College of New York, New York, New York*
[7]*Department of Psychology, Stanford University, Stanford, California*

Abstract: In-vivo measurements of human brain tissue conductivity at body temperature were conducted using focal electrical currents injected through intracerebral multicontact electrodes. A total of 1,421 measurements in 15 epileptic patients (age: 28 ± 10) using a radiofrequency generator (50 kHz current injection) were analyzed. Each contact pair was classified as being from healthy (gray matter, $n = 696$; white matter, $n = 530$) or pathological (epileptogenic zone, $n = 195$) tissue using neuroimaging analysis of the local tissue environment and intracerebral EEG recordings. Brain tissue conductivities were obtained using numerical simulations based on conductivity estimates that accounted for the current flow in the local brain volume around the contact pairs (a cube with a side length of 13 mm). Conductivity values were 0.26 S/m for gray matter and 0.17 S/m for white matter. Healthy gray and white matter had statistically different median impedances ($P < 0.0001$). White matter conductivity was found to be homogeneous as normality tests did not find evidence of multiple subgroups. Gray matter had lower conductivity in healthy tissue than in the epileptogenic zone (0.26 vs. 0.29 S/m; $P = 0.012$), even when the epileptogenic zone was not visible in the magnetic resonance image (MRI) ($P = 0.005$). The present in-vivo conductivity values could serve to create more accurate volume conduction models and could help to refine the identification of relevant intracerebral contacts, especially when located within the epileptogenic zone of an MRI-invisible lesion. *Hum Brain Mapp 38:974–986, 2017*.

Key words: electric conductivity; brain tissue; in-vivo measurement; volume conduction; depth electrode; stereoelectroencephalography; human investigation; epilepsy

*Correspondence to: Laurent Koessler, CRAN UMR 7039, CNRS - Université de Lorraine, 2 Avenue de la forêt de Haye, 54516 Vandoeuvre-lès-Nancy, France. E-mail: laurent.koessler@univ-lorraine.fr
Authors have no conflict of interest to declare.

Received for publication 17 April 2016; Revised 23 September 2016; Accepted 30 September 2016.
DOI: 10.1002/hbm.23431
Published online 11 October 2016 in Wiley Online Library (wileyonlinelibrary.com)

INTRODUCTION

Human brain tissue impedances are important parameters for determining the nature of volume conduction from an intra-cerebral source of neural activity to the scalp surface. Knowledge of these parameters (and their variability) is required in several domains such as electromagnetic source imaging [Haueisen et al., 2002; Vorwerk et al., 2014], transcranial direct current stimulation [Dmochowski et al., 2013], transcranial magnetic stimulation [Opitz et al., 2011; Salinas et al., 2009], electrical impedance tomography (EIT) [Abascal et al., 2008] and neuro-navigation [Johansson et al., 2009]. Two approaches have been developed to measure brain tissue impedances in humans. The first approach is the ex-vivo measurement of brain tissue impedance by passing current through tissue samples obtained during brain surgery [Skull: Akhtari et al., 2002; Geddes and Baker, 1967; Hoekema et al., 2003; Oostendorp et al., 2000; Cerebrospinal fluid (CSF): Baumann et al., 1997; Brain: Akhtari et al., 2006, 2010; Schmid et al., 2003; Gray matter: Gabriel et al., 1996]. The second approach is the in-vivo measurement using scalp EIT [Gibson et al., 2000; Gonçalves et al., 2003a,b; Grasso et al., 2002; Tidswell et al., 2001], magnetic resonance imaging (MRI) [Sekino et al., 2004], scalp EEG recordings [Baysal and Haueisen, 2004; Lai et al., 2005] or electrical intracerebral current injection [Latikka et al., 2001; Satzer et al., 2014]. The most common in-vivo approach relies on scalp EIT measurements that use electrical current injection through scalp sensors. This approach is limited by the fact that a large part of the applied scalp current is shunted through the scalp and skull, both of which are known to attenuate the amplitude of the signal [Koessler et al., 2015]. Moreover, scalp EIT is also burdened by the solution of an ill-posed non-linear inverse problem [Gonçalves et al., 2000].

To date, only one study [Latikka et al., 2001] has estimated conductivities using intracerebral measurements in humans. The in-vivo resistance of brain tissue was measured in healthy and pathological (tumors) human brain tissue. One limitation of this previous study is the limited number of measurements performed for each tissue type: only 21 measurements in white matter (WM) and 32 in gray matter were performed. This limit was due to a reliance on repeated impedance measurements from only one monopolar intracerebral contact per patient.

Abbreviations

EZ	epileptogenic zone
EIT	electrical impedance tomography
GM	gray matter
RF	radio frequency
R	reference resistance
r	intrinsic resistance
SEEG	stereoelectroencephalography
WM	white matter

The primary purpose of our study was to assess the in-vivo impedances and electric conductivities of human brain tissue (GM and WM) using focal electrical current injection through multicontact intracerebral electrodes. We also sought to determine whether healthy and pathological (epileptogenic) gray matter could be differentiated based on their impedances and whether tissue impedance varies with age.

MATERIALS AND METHODS

Patients

Fifteen patients (5 females) with partially refractory epilepsy aged from 16 to 50 years (mean: 28 years) (Table I) were prospectively investigated from October 2013 to June 2014. Prior to this study, all patients underwent a presurgical evaluation that included medical history, neuropsychological testing, 10/20 scalp EEG-video monitoring, electrical source imaging using 64-channel video-EEG recordings [Koessler et al., 2010], high resolution cranial MRI (voxel size: 1 mm^3), cranial fluorodeoxyglucose positron emission tomography (FDG-PET) study and simultaneous scalp and intracerebral EEG recordings. Seven patients had frontal lobe epilepsy, five had temporal lobe epilepsy, two had parietal lobe epilepsy, and one multifocal epilepsy. Three patients had dysplasia, three hippocampal sclerosis, one cortical tubers, one gyration abnormality, one gyration atrophy, and one periventricular heterotopia. In five patients, no lesion was visible in the MRI. Ten out of fifteen patients finally underwent surgery (Table I).

All patients provided informed consent prior to participation. The study was granted approval by the local research ethics committee CPP Est III (Clinical trial NCT 01090934).

Intracerebral Electrodes and Stereotactic Placement

Intracerebral electrodes, consisting of 5–15 contiguous contacts of 2 mm in length separated by 1.5 mm, were used to record intracerebral EEG signals during the presurgical investigation (DIXI Microtechniques, Besançon, France) (Fig. 1). The intracerebral electrodes had a diameter of 0.8 mm and lengths varying from 16 to 61.5 mm. The contacts were made of Platinum/Iridium (90/10) and the electrodes were isolated by polyamide material. These electrodes are designed for stereoelectroencephalography (SEEG) investigations [Talairach et al., 1974]. Placement of intracerebral electrodes relied on electroclinical hypotheses and were intended to define the epileptogenic zone to be surgically removed for epilepsy treatment and the surrounding tissues that cannot be removed without damaging necessary functionality [Maillard et al., 2009].

TABLE I. Main clinical features of all fifteen patients (P1–P15)

Patients	Age (year)	Epileptogenic zone	Lesion on MRI	Number of intracerebral contacts	Engel class
P1	23	L superior temporal gyrus	Gyration abnormality	100	–
P2	27	L mesial temporal	HS	103	IA
P3	44	L superior parietal lobule	No	103	–
P4	25	R precentral gyrus	Dysplasia	37	IA
P5	17	L superior parietal lobule	No	123	ID
P6	40	L mesial temporal	HS	124	IA
P7	16	R inferior frontal gyrus	No	196	IA
P8	17	R superior temporal gyrus and L anterior perisylvian	No	156	–
P9	23	L and R periventricular heterotopia	Periventricular heterotopia	162	–
P10	50	L mesial temporal	HS	122	IA
P11	30	L and R frontal	Cortical tubers	125	ID
P12	25	L frontal opercular	Dysplasia	105	IA
P13	38	R ventrolateral prefrontal cortex	Dysplasia	132	III
P14	22	L superior frontal sulcus	No	128	IA
P15	29	R mesial temporal	HS	125	–
Mean	**28**		Mean	**122**	

L, left; R, right; HS, hippocampal sclerosis.

Stereotactic placement of the intracerebral electrodes was performed as follows: First, electrode trajectories were defined using pre-operative MRI (3D T1 after gadolinium injection) with careful avoidance of vascular structures. Then, after induction of general anesthesia, a Leksell G-frame (Elekta SA, Stockholm, Sweden) was positioned on the patient's head and a stereotactic CT-scan was performed. Using a computer-assisted stereotactic software (Iplan stereotaxy, Brainlab, Feldkirchen, Germany) and CT-MR co-registration, the electrode trajectories were transformed from MR to Leksell frame-coordinates. For each intracerebral electrode, a guidance screw (internal diameter of 1 mm) was inserted into the skull according to the Leskell coordinates previously defined. Finally, each intracerebral electrode was inserted into the guidance screw and a sterile cap was immediately screwed onto it in order to fix the position of the intracerebral electrode, to avoid infectious complications and to prevent CSF leak. In our cohort, each patient had an average of 122 ± 35 intracerebral contacts (Table I). After implantation of intracerebral electrodes, a post-operative computed tomography (CT) scan was co-registered with the pre-surgical high resolution cranial MRI to precisely localize intracerebral contact positions. Due to the minimally invasive procedure used for SEEG, no brain swelling occurred [Cardinale et al., 2013; Mathon et al., 2015; Serletis et al., 2014; 863 procedures], leading to accurate and reliable MR-CT co-registration.

Radio Frequency Generator

A radio frequency (RF) generator (RFG-3C Plus, Radionics, Burlington, MA) was used to obtain tissue impedances (Fig. 1). This device is routinely used to induce StereoEEG-guided RF-thermo-lesions in the epileptogenic zone of drug-resistant epileptic patients [Guénot et al., 2011]. The device consists of a microprocessor-based lesion generator capable of supplying up to 50 W of RF power while continuously monitoring both the tissue impedance and the temperature. It also estimates the magnitude of the complex impedance vector Z:

$$|Z| = V_{\mathrm{rms}}/I_{\mathrm{rms}} \quad (1)$$

where V_{rms} and I_{rms} are the root mean square voltage and current measurements of a sinusoidal signal at 50 kHz frequency [Cosman and Cosman, 2005]. The magnitude of the impedance ($|Z|$) can be measured from 0 to 1,000 Ω with a resolution of 1 Ω.

Measurement of Intracerebral Electrode Impedance

Impedance measurements depend on electrode geometry and material as well as the electromagnetic properties of the surrounding tissues. We define R as the impedance due to the electrode geometry (including electromagnetic properties of intracerebral electrode) and r as the impedance due to the electrode material. R is herein termed the "reference resistance" and r the intrinsic resistance.

We first estimated R (reference resistance) by performing electrostatic analysis in the COMSOL Multiphysics 4.2 software (http://www.comsol.com) (Fig. 2). A finite element model was constructed to model the intracerebral electrodes and brain volume. For the brain, a spherical model with two different diameters: 180 and 160 mm was employed [Kuhlenbeck, 1973]. A homogeneous conductivity of

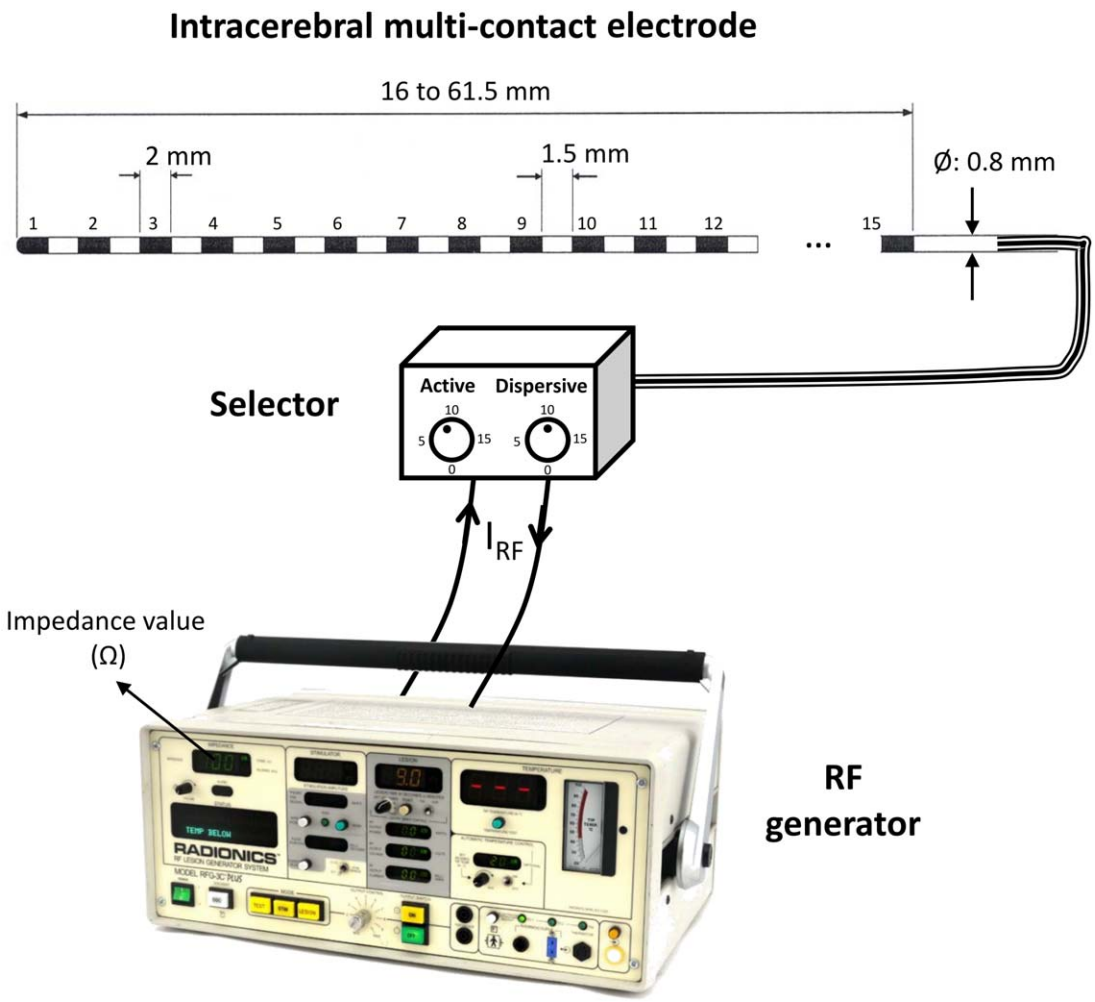

Figure 1.

Instrumental configuration for in-vivo brain tissue impedance measurements. Intracerebral multi-contact electrodes were connected to a selector device that determined the active and dispersive contacts. Impedance values were obtained via a RF generator that performed electrical current injection with a 50 kHz sinusoidal signal. [Color figure can be viewed at wileyonlinelibrary.com]

$\sigma_0 = 1$ S/m was set for the brain volume. Electrode contacts were modeled as platinum with a conductivity of $9.5e^6$ S/m. The spacing between contacts was modeled as polyamide with a conductivity of $1e^{-12}$ S/m. The impedance R was computed for every contiguous pair of intracerebral contacts (i.e., over the full electrode length), by starting from the first contacts located at tip of the intracerebral electrode and finishing with the last contacts next to the outer boundary of the spherical model (contacts 1–2, 2–3, 3–4 . . .). Computation was performed every 3.5 mm which corresponds to the mean distance between two contiguous platinum contacts. One contact was used as the current source ("boundary current source" in COMSOL) with a 1 A/m^2 magnitude and its neighbor contact was set to ground. After solving Maxwell's equation, we computed potentials and current streamlines were illustrated for visualization (Fig. 2). The R value was calculated as follows:

$$R = \frac{V_e}{\oint_A J.dA} \tag{2}$$

where, V_e is the average potential in the electrode produced by the current injection, and where the denominator is the integral of the current density across the electrode surface (J—current density vector field, A—boundary surface of an electrode, dA—vector area of surface A, directed as the surface norm). Given the dimensions of electrode contact and imposed current source (1 A/m^2), the integral of electrode surface density norms was 5.02 μA.

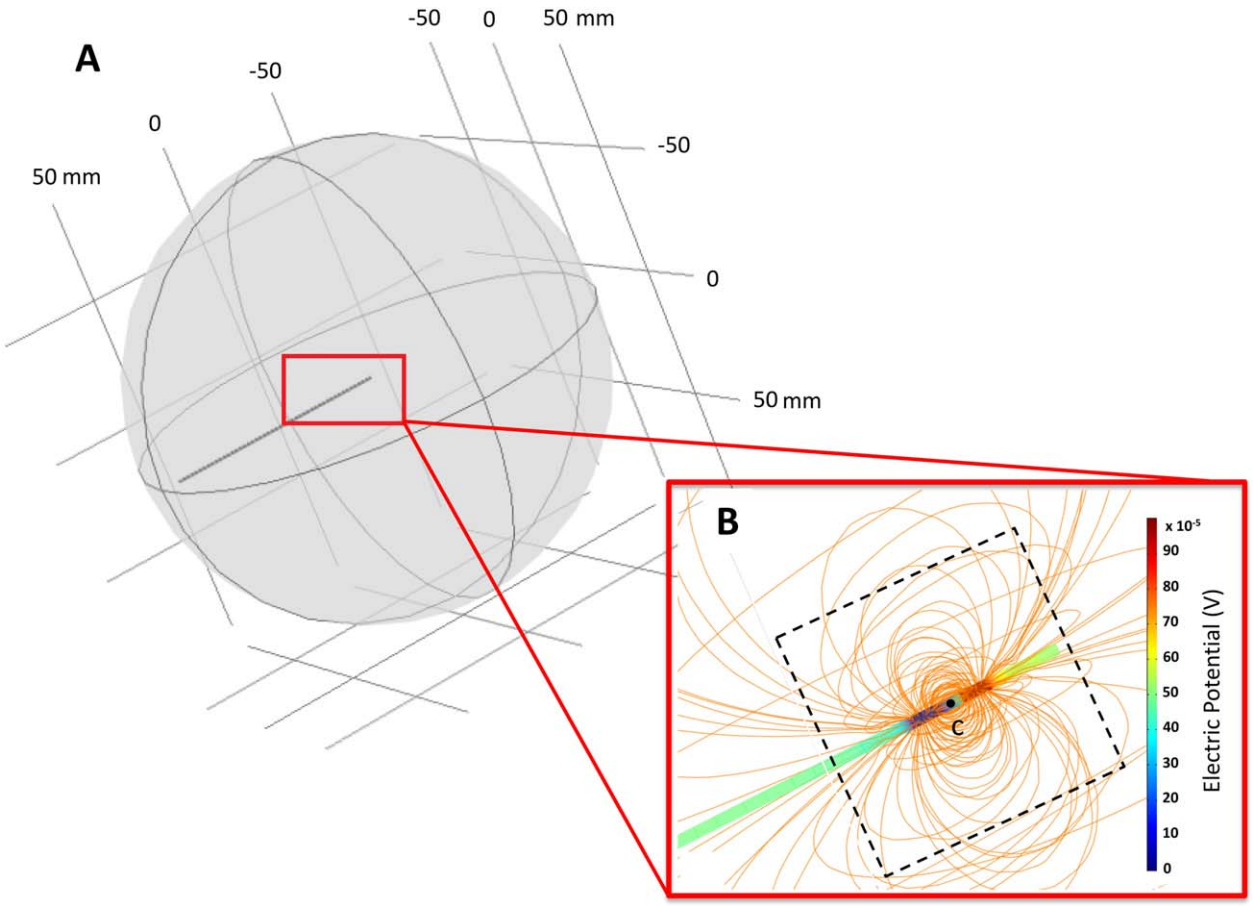

Figure 2.

(A) Comsol Multiphysics model with a 160 mm-diameter sphere and a 1 S/m-conductivity value for the calculation of geometrical impedance of an intracerebral electrode and (B) potential and current density streamlines of electrical stimulation between two contiguous contacts using boundary current source of 1 A/m^2. For volume-based conductivity estimation, tissue environment was explored in a cube with a side length of 13 mm (see dotted line; cube that includes more than 75% of current flow and four intracerebral contacts) centered on the middle (C) of intracerebral contact pairs. [Color figure can be viewed at wileyonlinelibrary.com]

Next, we measured *r* (intrinsic resistance) by performing empirical measurements with the RF generator. A 1 kΩ load resistor was plugged to two contiguous platinum contacts and an electrical current injection (50 kHz sinusoidal wave) from RF-generator was injected into these contacts (one active and one dispersive). Then, *r* value was obtained using the value given by the RF-generator less the value of the load resistor (1 kΩ).

Direct Estimation of Brain Tissue Impedances

For each patient, measurements of brain tissue impedances were performed two hours after the end of the surgical implantation. Special care was taken to include awake patients in this study. Intracerebral impedances were measured between successive platinum contacts (1–2, 2–3 ... 14–15) along each intracerebral electrode. The first contact was designated as the active electrode and the second as the dispersive electrode. Due to the short distance (2 mm) between active and dispersive electrode, current injection was assumed as focal. A selector switch, placed between the RF generator and intracerebral electrode, was used to select the active and dispersive contacts (Fig. 1).

From Tissue Impedances to Conductivity and Resistivity Values

For both sphere configurations used in numerical simulation (COMSOL Multiphysics 4.2), mean reference resistances were respectively 199.8 ± 1.3 Ω and 199.3 ± 0.2 Ω (Table II). Due to these similar mean values and their very low standard deviations, we used a single reference resistance *R* of 199.5 Ω.

TABLE II. Geometrical electrode impedances using numerical simulations

Geometrical electrode impedance (R) for a 160 mm-diameter brain					Geometrical electrode impedance (R) for a 180 mm-diameter brain				
Distance from the tip of electrode (mm)	Current norm (μA)	Electric potential (mV)	R (Ω)	Distance from outer boundary (mm)	Distance from the tip of electrode (mm)	Current norm (μA)	Electric potential (mV)	R (Ω)	Distance from outer boundary (mm)
0.0	5.02	1.003	199.56	80.0	0.0	5.02	1.001	199.25	90.0
3.5	5.02	1.003	199.57	76.5	3.5	5.02	1.001	199.23	86.5
7.0	5.02	1.002	199.52	73.0	7.0	5.02	1.001	199.29	83.0
10.5	5.02	1.003	199.57	69.5	10.5	5.02	1.001	199.21	79.5
14.0	5.02	1.003	199.55	66.0	14.0	5.02	1.001	199.33	76.0
17.5	5.02	1.002	199.51	62.5	17.5	5.02	1.002	199.36	72.5
21.0	5.02	1.003	199.59	59.0	21.0	5.02	1.001	199.21	69.0
24.5	5.02	1.002	199.47	55.5	24.5	5.02	1.001	199.25	65.5
28.0	5.02	1.002	199.54	52.0	28.0	5.02	1.002	199.35	62.0
31.5	5.02	1.003	199.61	48.5	31.5	5.02	1.001	199.25	58.5
35.0	5.02	1.002	199.47	45.0	35.0	5.02	1.001	199.29	55.0
38.5	5.02	1.002	199.49	41.5	38.5	5.02	1.001	199.24	51.5
42.0	5.02	1.003	199.55	38.0	42.0	5.02	1.001	199.23	48.0
45.5	5.02	1.003	199.55	34.5	45.5	5.02	1.001	199.27	44.5
49.0	5.02	1.002	199.44	31.0	49.0	5.02	1.001	199.26	41.0
52.58	5.02	1.002	199.48	27.5	52.58	5.02	1.001	199.30	37.5
56.0	5.02	1.002	199.54	24.0	56.0	5.02	1.001	199.33	34.0
59.5	5.02	1.003	199.60	20.5	59.5	5.02	1.001	199.32	30.5
63.0	5.02	1.002	199.53	17.0	63.0	5.02	1.001	199.26	27.0
66.5	5.02	1.003	199.72	13.5	66.5	5.02	1.001	199.24	23.5
70.0	5.02	1.006	200.32	10.0	70.0	5.02	1.001	199.33	20.0
73.5	5.02	1.033	205.64	6.5	73.5	5.02	1.002	199.40	16.5
		Mean	**199.86**		77.0	5.02	1.002	199.48	13.0
					80.5	5.02	1.006	200.20	9.5
							Mean	**199.33**	

Using the RF generator, the intrinsic resistance (r) due to electrode's material (platinum for contacts and polyamide for intercontacts), was measured as 159 Ω. These electrode resistances (combining R and r) were used to convert the measured brain tissue impedance into brain tissue conductivity. Conductivity was estimated using the following formula that take into account the electrode geometry and material:

$$\sigma = \sigma_0 * K; \text{ with } K = \frac{R}{(|Z|-r)} = \frac{199.5}{|Z|-159} \quad (3)$$

where σ was the conductivity (S/m), σ_0 the homogeneous conductivity used for simulation (1 S/m), K a constant, R the reference resistance due to electrode's geometry (199.5 Ω), $|Z|$ the measured impedance magnitude coming from RF-generator (Ω), and r the intrinsic resistance due to electrode's material (159 Ω). The resistivity value was defined as the inverse of conductivity.

Brain Tissue Classification for the Direct Estimation

As a first step, the position of each intracerebral contact was automatically detected in the individual CT-scan [Hofmanis et al., 2011] and then visually defined using individual MR-CT co-registration (Fig. 3A). According to the intensity level of the voxels that completely surrounded the intracerebral contact pairs (i.e., about 15 voxels just next to the contact pairs in the MR slice), the measurement sites were classified as gray matter (GM) or white matter (WM). If more than one tissue type was identified in these measurement sites, measurements were discarded.

In a second step, the classification of brain tissue was validated using intracerebral EEG recordings. Using a bipolar EEG montage that provided the potential difference between two contiguous contacts, we analyzed intracerebral EEG activity (LGM and LK) (Fig. 3B). Intracerebral contacts that recorded physiological EEG activity were validated as comprising the GM class whereas those which recorded no activity were assigned to the WM class. Intracerebral contacts located in the GM that were involved at the onset of the initial ictal discharge were classified as being in the epileptogenic zone (EZ) class [Kahane et al., 2006]. In 10 out of 15 patients, a structural lesion was visible in MRI and belonged to the epileptogenic zone, while in the remaining 5 patients no structural lesion could be identified (MR-invisible epileptogenic zone).

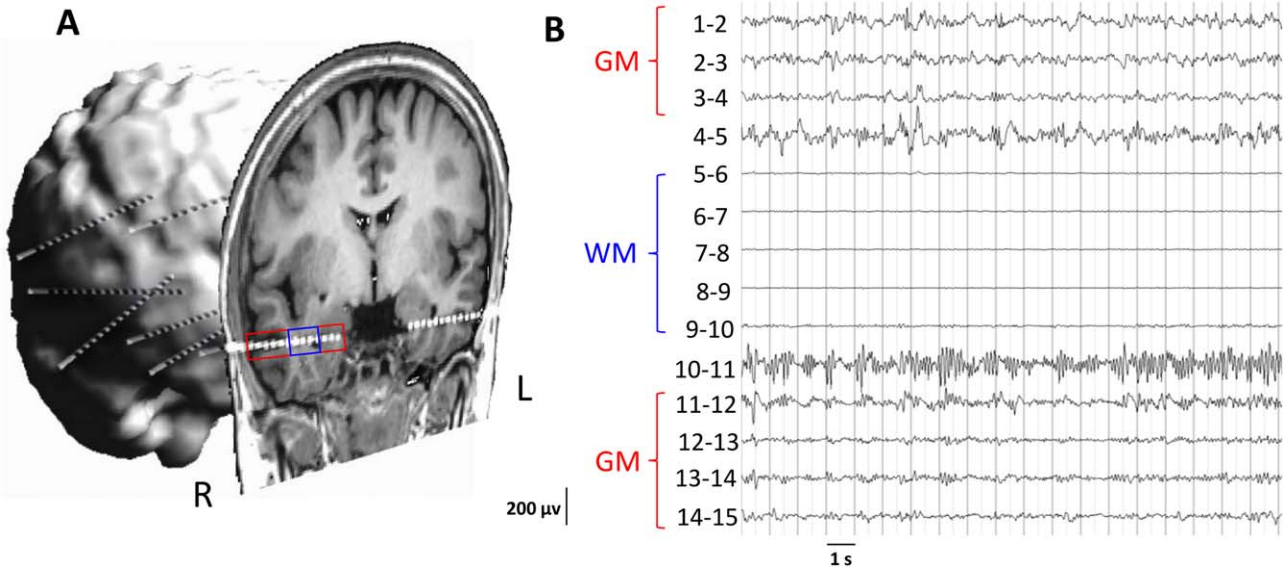

Figure 3.

Brain tissue characterization using individual (A) MR-CT co-registration and (B) intracerebral EEG recordings. Brain tissues were classified using (i) expert visual classification of automatically detected intracerebral contacts within the brain volume and (ii) electrophysiological measurements between two contiguous intracerebral contacts using stereroelectroencephalographic recordings. In this figure, intracerebral contacts that recorded normal physiological brain activity (i.e., without any pathological biomarkers) are indicated in red and were classified in the gray matter class. Intracerebral contacts that did not record any brain activity are indicated in blue and were classified in the white matter class. Electrode pairs giving strong signal at the edge between GM and WM (derivations 4–5 and 10–11) were discarded from the impedance analysis. [Color figure can be viewed at wileyonlinelibrary.com]

When there was a disagreement between MRI and electrophysiological classification (e.g., WM for MR classification and GM for SEEG classification), measurements were discarded.

Volume-Based Estimation of Brain Tissue Impedances

The aim of the volume-based estimation was to estimate the influence of the wider tissue environment on conductivity estimation. Using numerical simulation (source of 1 mA, conductivity 1 S/m; COMSOL Multiphysics 4.2), we estimated the current density norm and the percentage of current flow in different geometric planes (radius: 2, 4, 6, 8, 15, 20 mm) centered in the middle of the contact pairs (Fig. 2B). In these six planes, the percentages of confined current flow were, respectively, 45%, 62%, 74%, 81%, 91%, and 95%.

The spatial coordinates of the intracerebral contacts (see section "Brain tissue classification for the direct estimation") were used to calculate the center coordinates of all contact pairs in each patient. Then individual patient GM, WM, and CSF compartments were obtained using a unified segmentation and surface extraction of the presurgical anatomical MRI [Ashburner and Friston, 2005]. Finally, we determined the percentage of voxels defined as GM, WM and CSF in a cube with a side length of 13 mm centered on each intracerebral contact pair. This search was over 6 mm in all 3 directions around the centroid (1 mm) voxel and included at least 74% of the current flow and four intracerebral contacts instead of the two as were used in the direct estimation. When one or more voxels defined as being in the EZ were included in a cube, the measurements were discarded. Taking into account the current flow in this brain volume $(13\ \text{mm})^3$, we assumed that the measured impedance was equal to the sum of the impedances in series weighted by a coefficient that corresponds to the number of voxels from each class (GM and WM). We thus estimated each brain tissue impedance by solving a set of linear equations in two unknowns:

$$Z_{\text{meas}} = P_{\text{GM}} * Z_{\text{GM}} + P_{\text{WM}} * Z_{\text{WM}} \quad (4)$$

where Z_{meas} is the measured impedance (in Ω), Z_{GM}, Z_{WM} the two unknown impedances (in Ω) and P_{GM}, P_{WM}, the percentages of GM, WM voxels in the a cube with a side length of 13 mm centered on the intracerebral contact pairs. Goodness of fit was computed (1 – residual variance) in order to estimate the reliability of the volume-based estimation as compared with the direct estimation.

Statistical Analysis of Brain Tissue Impedances

The Shapiro–Wilk test [Shapiro and Wilk, 1965] was used to determine whether the impedances of each class

TABLE III. Brain tissue impedances, conductivities, and resistivities

	Gray matter (GM)			White matter (WM)			Epileptogenic zone (EZ)		
Patient	Mean (Ω)	SD	*n*	Mean (Ω)	SD	*n*	Mean (Ω)	SD	*n*
P1	920	160	41	1,263	124	31	887	79	7
P2	966	225	29	1,215	121	18	854	167	22
P3	899	290	43	1,383	351	30	537	142	9
P4	929	210	13	1,407	284	3	793	251	9
P5	1,050	184	39	1,288	176	40	690	220	20
P6	861	166	61	1,037	167	16	873	191	17
P7	898	177	70	1,239	123	64	862	144	15
P8	967	256	62	1,215	206	26	952	184	26
P9	904	140	68	1,093	131	69	974	87	10
P10	883	179	37	1,124	141	31	817	241	14
P11	997	281	55	1,320	144	49	755	210	7
P12	839	123	48	1,195	127	30	1,019	28	3
P13	855	125	44	1,250	99	47	1,018	114	4
P14	881	163	43	1,086	133	51	903	221	7
P15	842	101	43	1,059	94	25	865	123	25
Mean impedance (Ω)	**911**	**199**		**1,202**	**184**		**845**	**201**	
Mean conductivity (S/m)	**0.26**	**0.06**		**0.19**	**0.03**		**0.29**	**0.07**	
Mean resistivity (Ω · m)	**3.78**	**0.80**		**5.24**	**0.81**		**3.45**	**0.82**	

followed a normal distribution. As a first step, a Mann–Whitney *U* test was calculated between two impedance classes under the null hypothesis (H_0) that the impedances of healthy tissue (GM and WM) had identical median values. The significance level was set at $\alpha = 0.05$.

In addition, we checked for anisotropy in our WM data using exploratory data analysis tools (Shapiro–Wilk and Jarque–Bera normality tests, normal probability plot, histogram, and *K*-means clustering). In case of tissue anisotropy, we assumed that these tools would be able to identify two (or multiple) subsets of impedance in the WM class.

We also compared impedances of healthy GM with pathological GM (i.e., EZ) and then we compared healthy GM with MR-invisible EZ that corresponds to a subclass of pathological GM.

In addition, we studied the influence of patient age on the GM and WM impedances. Correlation coefficient and coefficients of determination were calculated to measure the strength of a linear association between patients' age and tissue impedance. We then computed the statistical *t* value under the null hypothesis (H_0) that there was no relationship between age and brain tissue impedance.

RESULTS

Brain Tissue Impedances and Resulting Conductivities Using Direct Estimation

Across 1,802 measurements in 15 patients, 381 were discarded due to the absence of concordance between MRI and intracerebral EEG recordings or the presence of more than one tissue in the environment of the intracerebral contact pairs. Among the 1,421 remaining measurements, 696 brain sites were classified as GM (mean: 46/patient), 530 as WM (mean: 35/patient) and 195 as EZ (mean: 13/patient) (Table III). Mean measured impedances were: GM: 911 ± 199 Ω; WM: $1{,}202 \pm 184$ Ω; EZ: 845 ± 201 Ω; (Table III, Fig. 4). Taking into account the realistic model of intracerebral electrodes (geometry and materials) and the use of Eq. (3), the resulting conductivities and resistivities for each class were: GM: 0.26 ± 0.06 S/m, 3.78 ± 0.80 Ω · m; WM: 0.19 ± 0.03 S/m, 5.24 ± 0.81 Ω · m; EZ: 0.29 ± 0.07 S/m, 3.45 ± 0.82 Ω · m (Table III). In the subclass of MR-invisible EZ, measured impedance was 813 ± 232 Ω. The respective resulting conductivity and resistivity was 0.30 ± 0.09 S/m and 3.29 ± 0.94 Ω · m.

GM, WM, and EZ impedances did not follow a normal distribution (Shapiro–Wilk test; $0.046 < P < 0.0001$). Pairwise comparisons showed that GM and WM had statistically different median impedances ($P < 0.0001$, Mann–Whitney *U* test). Additionally we showed that healthy GM had statistically higher median impedances than the epileptogenic zone ($P = 0.012$), even in cases of MR invisible EZ ($P = 0.005$) (Table IV).

Brain Tissue Impedances and Resulting Conductivities Using Volume-Based Estimation

Across 1,421 measurements, 220 measurements were discarded because more than 10% of the voxels in the cubes with a side length of 13 mm were not identified as GM, WM and CSF. Additionally, 516 measurements were discarded because more than 5% was defined as CSF. Across the 685 remaining measurements, we found an

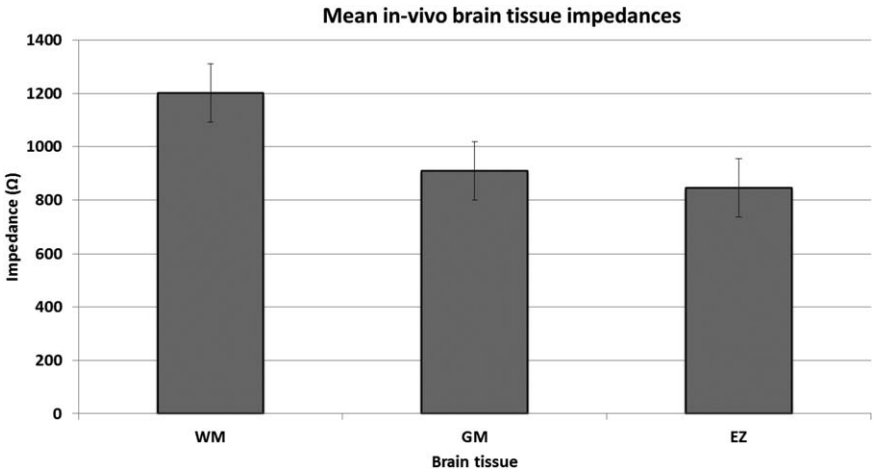

Figure 4.
Mean in-vivo brain tissue impedance values (in Ω) with confidence intervals (vertical lines) in a population of fifteen young adults (age: 28 ± 10 years) using a total of 1,421 measurements. WM, white matter; GM, gray matter; EZ, epileptogenic zone.

average of 51% and 49% of voxels in GM and WM compartments (standard deviation of 23% and 24% voxels, respectively). The impedances and resulting conductivities were respectively: GM: 912 Ω and 0.26 S/m; WM: 1365 Ω and 0.17 S/m with a goodness of fit of 89%.

White Matter Anisotropy and Correlation between Impedance and Patient's Age

Using the 530 measurements defined as WM, exploratory data analysis did not support the presence of more than one subgroup in the WM subset ($P \ll 0.01$ for normality tests). There was no correlation between brain tissue impedance obtained using measured impedances (RF generator) and patient's age: $r = -0.41$, $r^2 = 0.17$ and $t = 1.64$ for GM; $r = -0.09$, $r^2 = 0.01$ and $t = 0.33$ for WM; for a $t_{5\%}$ of 2.16) (Fig. 5).

DISCUSSION

In this study, we performed in-vivo impedance measurements of healthy and pathological brain tissues using focal electrical current injection through intracerebral multicontact electrodes.

In contrast to the most common in-vivo method (scalp EIT) based on scalp electrical current injection and impedance measurements, the intracerebral approach avoids uncertainties related to solving the inverse problem and associated biophysical head modeling. Secondly, the intracerebral approach is very efficient in characterizing different brain compartments such as GM and WM. Invasive approaches have been used for many years in animal or ex-vivo tissues [Crile et al., 1922; Freygang and Landau, 1955; Logothetis et al., 2007; Nicholson, 1965; Van Harreveld et al., 1963]. In such situations, several techniques have been developed to control the brain tissue environment [temperature, chemical substance, stress, and hypoxia; Crile et al., 1922; Freygang and Landau, 1955, Van Harreveld et al., 1963], to avoid electrode polarization, to adapt current sources and recordings [4-point measurement method; Logothetis et al., 2007], to control brain tissue geometry (histology) and to investigate questions of anisotropy (white matter especially). Our human in-vivo brain tissue investigation could not as carefully control some of these factors, especially the current injection and tissue identification steps. This is due to several factors including medical constraints (drug resistant epilepsy) and experimental conditions (in-vivo measurements) as well as the design of our intracerebral electrode design (2-point measurements) and placement and finally our RF generator characteristics. Nevertheless, in our study, all intracerebral contacts placed in different brain tissues were located within the brain volume using a novel approach that combined two different methods. Firstly, we performed an automated individual CT-MRI co-registration and a tissue identification using expert visual analysis. Secondly, we used intracerebral EEG recordings to optimize the

TABLE IV. Statistical analysis of brain tissue impedances

	Mann–Whitney *U* test
	P-value
GM–WM	<0.0001
GM–EZ	0.012
GM–MR invisible EZ	0.005

GM, gray matter; WM, white matter; EZ, epileptogenic zone.

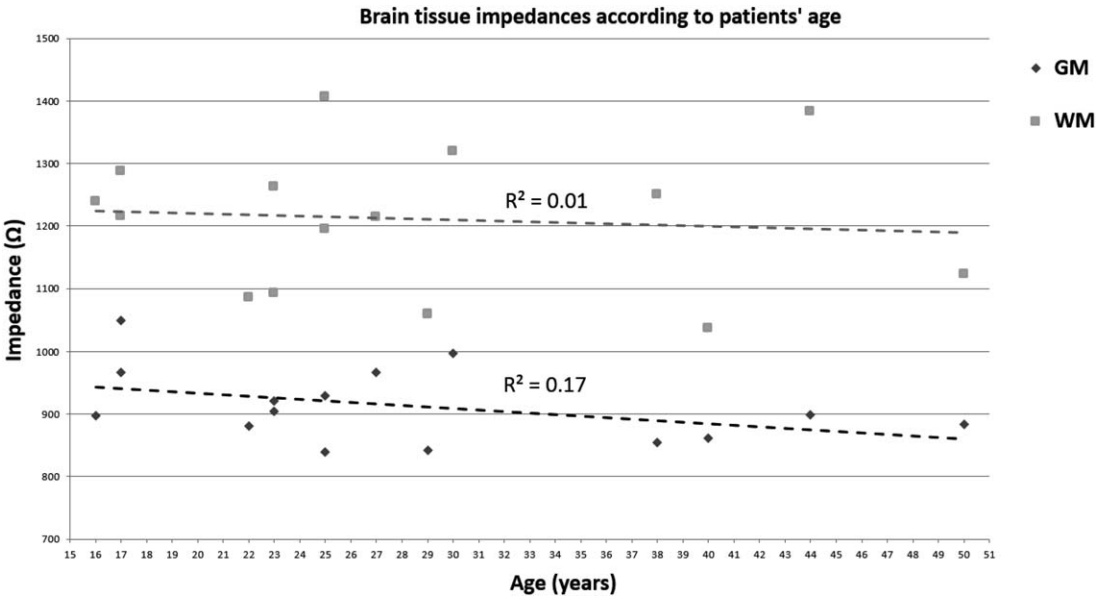

Figure 5.

Distribution of brain tissue impedances according to patients' age. There was no relationship between age and brain tissue impedance (t value was about 0.95 for age—GM and 0.60 for age—WM; $t_{5\%}$ of 2.16).

classification and definition of healthy or pathological brain tissue. Intracerebral EEG recordings are particularly crucial because pathological tissues (and their boundaries) are not consistently visible in MR images [Latikka et al., 2001] and thus could be falsely identified as healthy tissue. The 33% proportion of MR-invisible EZs in our cohort was comparable to that of adult patients with refractory focal epilepsy [McGonigal et al., 2007; Rikir et al., 2014].

Moreover, in addition to a visual analysis of the local tissue environment surrounding the intracerebral contact pairs, we developed an automated method that characterized a wider tissue environment. Using individual MR segmentation and tissue extraction, this method calculated for each measurement the percentage of a given tissue type within a cube with a side length of 13 mm centered on intracerebral contact pairs. Volume-based impedance estimation that relied on this geometric control method, gave similar results as the direct estimation (respectively GM: 0.26 vs. 0.26 S/m; WM: 0.17 vs. 0.19 S/m). Despite the anatomically structured tissues and the complexity of measuring in-vivo, the goodness of fit of volume-based estimation (89%) is quite good. Finally, the volume-based estimates confirm that our direct measurements using focal current injection through intracerebral contact pairs indeed investigated the local tissue environment.

The resistivity values (3.78 for GM and 5.24 $\Omega \cdot m$ for WM) obtained using direct estimation and the estimate of intracerebral electrode resistance (intrinsic and reference) are slightly higher than those reported in previous in-vivo scalp EIT studies: 2.45–3.01 $\Omega \cdot m$ in Gonçalves et al. [2003a,b] (6 subjects); 2.83 $\Omega \cdot m$ in Baysal and Haueisen [2004] (9 subjects). This is also slightly higher than the values reported in the only previous intracerebral study [Latikka et al., 2001]: 3.51 (GM) and 3.91 (WM) $\Omega \cdot m$ (53 measurements). In addition to this difference of the nature of measurements (in-vivo for our study versus ex-vivo), the frequency of electrical current injection (50 kHz for this study vs. 5–1,005 Hz) could explain this difference. Our GM and WM conductivities (respectively, 0.26 and 0.19 S/m) are consistent with previous ex-vivo estimates made at body temperature in humans [0.15–0.25 S/m at 37°C; Akhtari et al., 2006] but are slightly different from animal conductivity values [0.13–0.23 S/m, Crile et al., 1922; 0.10 S/m, Van Harreveld et al., 1963; 0.25–0.60 S/m, Logothetis et al., 2007].

Our study is the first to show significantly different impedances between GM and WM. This is likely due to a high number of measurements (1,421; 95 measurements/patient in average using direct estimation and 865; 58 measurements/patient using volume-based estimation) compared with the only previous intracerebral study [53 measurements in all; Latikka et al., 2001]. The absence of several subgroups in white matter subset is likely due to the trajectories of our intracerebral electrodes in radial, tangential and oblique directions. By taking into account the different orientations of WM fiber tracts in the brain and the different trajectories of our intracerebral electrodes, we measured WM impedances both in parallel and orthogonal directions. So, our methodology did not favor one direction over another.

The main limitation of our study is related to the high frequency of injected electrical current (50 kHz) which is above the frequency range of physiological EEG background activity (<250 Hz). The influence of the frequency of current injection on in-vivo human brain impedance is not well understood. The previous studies that investigated this frequency dependence used ex-vivo animal and human tissues [Gabriel et al., 1996; Faes et al., 1999]. At relatively low frequencies (<100 Hz), the permittivity of tissue can be disregarded and so only resistivity needs to be taken into account (quasi-static approach) [Gabriel et al., 1996]. In the higher frequency range (from 100 Hz to 100 kHz), conductivity values are higher. Our method could slightly overestimate in-vivo brain conductivity values (offset) due to the non-quasi-static situation. Taking into account brain tissue conductivities (0.3 S/m), the frequency of current injection (50 kHz) and the maximum radius of human head (0.13 m), propagation and inductive effects can be neglected whereas capacitive effects cannot be neglected according to the criteria defined in Plonsey and Heppner, [1967] [effect values $\ll 1$; Eqs. from (21) to (24)]. However, in Gabriel et al. [1996] and Faes et al. [1999] tissue conductivity remained stable between 100 Hz and 100 kHz thus suggesting that these values are still valid for electrophysiological activity (<250 Hz).

The second limitation concerns our mixture model [Eq. (4)] of a linear sum that relies on the hypothesis that the different tissues were connected in series between the two contacts. We could have made an alternative hypothesis that these tissues were connected in parallel. This would result in a lower overall resistivity than the serial connection in the same volume. In our study, this alternative hypothesis is unlikely because it would assume that intracerebral multicontact electrodes would have to lie precisely inside a boundary between two tissues throughout. We cannot completely exclude this hypothesis and we have to mention that our conductivity values may be slightly underestimated due to the assumption of serial connection. Finally, the last limitation concerns the two-hour delay between the general anesthesia and the impedance measurements. This delay was intended to preserve the routine post-operative intracerebral EEG recordings. According to the short half-life of propofol used for all patients (30–60 min), the effect of the hypnotic agent can be considered as non-significant.

Knowledge of brain tissue conductivities is especially important for head modeling in electromagnetic source imaging [Akhtari et al., 2010; Birot et al., 2014]. Our study confirms that the brain cannot be considered as an electrically homogeneous volume, supporting the use of finite element models in source imaging studies. Several studies [Güllmar et al., 2010; Hallez et al., 2008; Wolters et al., 2006] have demonstrated that an incorrect specification of brain conductivity induces errors in calculations of electrical forward solutions and electromagnetic source localizations. Despite this, most source localization studies use a nominal isotropic value for brain conductivity (0.33 S/m for both GM and WM) coming from ex-vivo investigation of brain tissue after long post-mortem delays at very high frequency stimulation (800–2,450 MHz) [Schmid et al., 2003] or indirect measurement with scalp EIT/EEG investigation [Gonçalves et al., 2003a, b; Baysal and Haueisen, 2004]. Our study provides new values for in-vivo brain tissue conductivity that should be closer to the physiological values required for electrical source imaging studies. In addition, these new values could be employed in simulations of the electric field generated by non-invasive brain stimulation (tDCS and TMS). In such situations, the current injected through scalp electrodes induces an electric field in the space near the injection site and also at brain tissue surfaces with different electrical conductivities [Tofts and Branston, 1991]. Salinas et al. [2009] demonstrated that this electric field (especially its magnitude and direction) cannot be estimated without an accurate description of the tissue conductivity values.

We found no relation in our young adult population between patients' age and GM or WM impedances ($0.33 < t < 1.64$, $t_{5\%} = 2.16$). Moreover, our gray and white matter impedances are in the same range of impedances as Latikka et al.'s who investigated an older cohort with an average age of 59.9 ± 15 years. By consequence, our resistivity/conductivity values could be used as a reference for all young human adults.

Concerning pathological brain tissue impedances, we investigated epileptogenic zones defined by intracerebral EEG recordings. Mean EZ resistivity was about 3.45 $\Omega \cdot$m which is lower than WM and GM impedances. EZ impedances were statistically different from healthy gray matter impedances (EZ vs. GM: $P = 0.012$) even in cases of MR invisible EZ ($P = 0.005$).

Intracerebral impedance investigation could be a promising tool for the delineation of EZ especially in this subclass of MR-invisible EZ that represents a challenge for epilepsy surgery. As far as we know, epileptogenic tissue impedance and conductivity have not been reported until now. This specific high EZ conductivity value could be used as a clinical biomarker to confirm the electrophysiological findings of SEEG recordings and to plan the extent of thermal lesions (i.e., the number of intracerebral contacts used for thermocoagulation). The use of impedance measurements as biomarkers already exists in other applications like deep brain surgery, brain tumors and arteriovenous malformation localizations and chronic stroke diagnosis [Johansson et al., 2009; Romsauerova et al., 2006; Siemionow et al., 2000].

CONCLUSION

Across 1,421 measurements in a population of fifteen young adults, we demonstrated that gray and white matter tissue had statistically different in-vivo impedances at 50 kHz frequency current injection. Gray matter had

higher median impedances in healthy tissue than in the epileptogenic zone, even in cases of MR invisible epileptogenic zone. No effect of age on cerebral impedances was observed in our cohort. To conclude, in-vivo impedance measurements of cerebral tissues should be used for modeling volume conduction models in electromagnetic source imaging. Our results should prompt new studies assessing the diagnostic value of brain tissue impedance measurement for the identification and delineation of the epileptogenic zone.

ACKNOWLEDGMENTS

This study was supported in part by the Regional Council of Lorraine.

REFERENCES

Abascal JF, Arridge SR, Atkinson D, Horesh R, Fabrizi L, De Lucia M, Horesh L, Bayford RH, Holder DS (2008): Use of anisotropic modelling in electrical impedance tomography: Description of method and preliminary assessment of utility in imaging brain function in the adult human head. Neuroimage 43:258–268.

Akhtari M, Bryant HC, Mamelak AN, Flynn ER, Heller L, Shih JJ, Mandelkern M, Matlachov A, Ranken DM, Best ED, DiMauro MA, Lee RR, Sutherling WW (2002): Conductivities of three-layer live human skull. Brain Topogr 14:151–167.

Akhtari M, Salamon N, Duncan R, Fried I, Mathern GW (2006): Electrical conductivities of the freshly excised cerebral cortex in epilepsy surgery patients; correlation with pathology, seizure duration, and diffusion tensor imaging. Brain Topogr 18: 281–290.

Akhtari M, Mandelkern M, Bui D, Salamon N, Vinters HV, Mathern GW (2010): Variable anisotropic brain electrical conductivities in epileptogenic foci. Brain Topogr 23:292–300.

Ashburner J, Friston KJ (2005): Unified segmentation. Neuroimage 26:839–851.

Baumann SB, Wozny DR, Kelly SK, Meno FM (1997): The electrical conductivity of human cerebrospinal fluid at body temperature. IEEE Trans Biomed Eng 44:220–223.

Baysal U, Haueisen J (2004): Use of a priori information in estimating tissue resistivities -application to human data in vivo. Physiol Meas 25:737–748.

Birot G, Spinelli L, Vulliémoz S, Mégevand P, Brunet D, Seeck M, Michel CM (2014): Head model and electrical source imaging: A study of 38 epileptic patients. Neuroimage Clin 16:77–83.

Cardinale F, Cossu M, Castana L, Casaceli G, Schiariti MP, Miserocchi A, Fuschillo D, Moscato A, Caborni C, Arnulfo G, Lo Russo G (2013): Stereoelectroencephalography: Surgical methodology, safety, and stereotactic application accuracy in 500 procedures. Neurosurgery 72:353–366.

Cosman ER, Jr, Cosman ER Sr (2005): Electric and thermal field effects in tissue around radiofrequency electrodes. Pain Med 6: 405–424.

Crile GW, Hosmer HR, Rowland AF (1922): The electrical conductivity of animal tissues under normal and pathological conditions. Am J Physiol 60:59–106.

Dmochowski JP, Datta A, Huang Y, Richardson JD, Bikson M, Fridriksson J, Parra LC (2013): Targeted transcranial direct current stimulation for rehabilitation after stroke. Neuroimage 15:12–19.

Faes TJ, van der Meij HA, de Munck JC, Heethaar RM (1999): The electric resistivity of human tissues (100 Hz-10 MHz): a meta-analysis of review studies. Physiol Meas 20:R1–10.

Freygang WH, Landau WM (1955): Some relations between resistivity and electrical activity in the cerebral cortex of the cat. J Cell Comp Physiol 45:377–392.

Gabriel S, Lau RW, Gabriel C (1996): The dielectric properties of biological tissues: II. Measurements in the frequency range 10 Hz to 20 GHz. Phys Med Biol 41:2251–2269.

Geddes LA, Baker LE (1967): The specific resistance of biological material - a compendium of data for the biomedical engineer and physiologist. Med Biol Eng 5:271–293.

Gibson A, Bayford RH, Holder DS (2000): Two-dimensional finite element modelling of the neonatal head. Physiol Meas 21: 45–52.

Gonçalves S, de Munck JC, Heethaar RM, Lopes da Silva FH, van Dijk BW (2000): The application of electrical impedance tomography to reduce systematic errors in the EEG inverse problem - a simulation study. Physiol Meas 21:379–393.

Gonçalves S, de Munck JC, Verbunt JP, Bijma F, Heethaar RM,L da Silva FH (2003a): In vivo measurement of the brain and skull resistivities using an EIT-based method and realistic models for the head. IEEE Trans Biomed Eng 50:754–767.

Gonçalves S, de Munck JC, Verbunt JP, Heethaar RM, da Silva FH (2003b): In vivo measurement of the brain and skull resistivities using an EIT-based method and the combined analysis of SEF/SEP data. IEEE Trans Biomed Eng 50:1124–1128.

Grasso G, Alafaci C, Passalacqua M, Morabito A, Buemi M, Salpietro FM, Tomasello F (2002): Assessment of human brain water content by cerebral bioelectrical impedance analysis: A new technique and its application to cerebral pathological conditions. Neurosurgery 50:1064–1072.

Guénot M, Isnard J, Catenoix H, Mauguière F, Sindou M (2011): SEEG-guided RF-thermocoagulation of epileptic foci: A therapeutic alternative for drug-resistant non-operable partial epilepsies. Adv Tech Stand Neurosurg 36:61–78.

Güllmar D, Haueisen J, Reichenbach JR (2010): Influence of anisotropic electrical conductivity in white matter tissue on the EEG/MEG forward and inverse solution. A high-resolution whole head simulation study. Neuroimage 51:145–163.

Hallez H, Vanrumste B, Van Hese P, Delputte S, Lemahieu I (2008): Dipole estimation errors due to differences in modeling anisotropic conductivities in realistic head models for EEG source analysis. Phys Med Biol 53:1877–1894.

Haueisen J, Tuch DS, Ramon C, Schimpf PH, Wedeen VJ, George JS, Belliveau JW (2002): The influence of brain tissue anisotropy on human EEG and MEG. Neuroimage 15:159–166.

Hoekema R, Wieneke GH, Leijten FSS, van Veelen CWM, van Rijen PC, Huiskamp GJM, Ansems J, van Huffelen AC (2003): Measurement of the conductivity of skull. Temporarily removed during epilepsy surgery. Brain Topogr 16:29–38.

Hofmanis J, Caspary O, Louis-Dorr V, Maillard L (2011): Automatic depth electrode localization in intracranial space. 4th International Conference on Bio-inspired Systems and Signal Processing, *Biosignals* 2011. Rome, Italy.

Johansson JD, Blomstedt P, Haj-Hosseini N, Bergenheim AT, Eriksson O, Wardell K (2009): Combined diffuse light reflectance and electrical impedance measurements as a navigation aid in deep brain surgery. Stereotact Funct Neurosurg 87: 105–113.

Kahane P, Landré E, Minotti L, Francione S, Ryvlin P (2006): The Bancaud and Talairach view on the epileptogenic zone: A working hypothesis. Epileptic Disord 8:S16–S26.

Kuhlenbeck H (1973): Overall morphologic pattern Vol. 3/II. In: Karger S, editor. The Central Nervous System of Vertebrates. Basel. 950 p.

Koessler L, Benar C, Maillard L, Badier JM, Vignal JP, Bartolomei F, Chauvel P, Gavaret M (2010): Source localization of ictal epileptic activity investigated by high resolution EEG and validated by SEEG. Neuroimage 51:642–653.

Koessler L, Cecchin T, Colnat-Coulbois S, Vignal JP, Jonas J, Ramantani G, Vespignani H, Maillard L (2015): Catching the invisible: Mesial temporal source contribution to simultaneous EEG and SEEG recordings. Brain Topogr 28:5–20.

Lai Y, van Drongelen W, Ding L, Hecox KE, Towle VL, Frim DM, He B (2005): Estimation of in vivo human brain-to-skull conductivity ratio from simultaneous extra- and intra-cranial electrical potential recordings. Clin Neurophysiol 116:426–465.

Latikka J, Kuurne T, Eskola H (2001): Conductivity of living intracranial tissues. Phys Med Biol 46:1611–1616.

Logothetis NK, Kayser C, Oeltermann A (2007): In vivo measurement of cortical impedance spectrum in monkeys: Implications for signal propagation. Neuron 55:809–823.

Maillard L, Koessler L, Colnat-Coulbois S, Vignal JP, Louis-Dorr V, Marie PY, Vespignani H (2009): Combined SEEG and source localisation study of temporal lobe schizencephaly and polymicrogyria. Clin Neurophysiol 120:1628–1636.

Mathon B, Clemenceau S, Hasboun D, Habert MO, Belaid H, Nguyen-Michel VH, Lambrecq V, Navarro V, Dupont S, Baulac M, Cornu P, Adam C (2015): Safety profile of intracranial electrode implantation for video-EEG recordings in drug-resistant focal epilepsy. J Neurol 262:2699–2712.

McGonigal A, Bartolomei F, Régis J, Guye M, Gavaret M, Trébuchon-Da Fonseca A, Dufour H, Figarella-Branger D, Girard N, Péragut JC, Chauvel P (2007): Stereoelectroencephalography in presurgical assessment of MRI-negative epilepsy. Brain 130:3169–3183.

Nicholson PW (1965): Specific impedance of cerebral white matter. Exp Neurol 13:386–401.

Oostendorp TF, Delbeke J, Stegeman DF (2000): The conductivity of the human skull: Results of in vivo and in vitro measurements. IEEE Trans Biomed Eng 47:1487–1492.

Opitz A, Windhoff M, Heidemann RM, Turner R, Thielscher A (2011): How the brain tissue shapes the electric field induced by transcranial magnetic stimulation. Neuroimage 58:849–859.

Plonsey R, Heppner DB (1967): Considerations of quasi-stationarity in electrophysiological systems. Bull Math Biophys 29:657–664.

Rikir E, Koessler L, Gavaret M, Bartolomei F, Colnat-Coulbois S, Vignal JP, Vespignani H, Ramantani G, Maillard LG (2014): Electrical source imaging in cortical malformation-related epilepsy: A prospective EEG-SEEG concordance study. Epilepsia 55:918–932.

Romsauerova A, McEwan A, Horesh L, Yerworth R, Bayford RH, Holder DS (2006): Multi-frequency electrical impedance tomography (EIT) of the adult human head: Initial findings in brain tumours, arteriovenous malformations and chronic stroke, development of an analysis method and calibration. Physiol Meas 27:147–161.

Salinas FS, Lancaster JL, Fox PT (2009): 3D modeling of the total electric field induced by transcranial magnetic stimulation using the boundary element method. Phys Med Biol 54: 3631–3647.

Satzer D, Maurer EW, Lanctin D, Guan W, Abosch A (2014): Anatomic correlates of deep brain stimulation electrode impedance. J Neurol Neurosurg Psychiatry 86:398–403.

Schmid G, Neubauer G, Mazal PR (2003): Dielectric properties of human brain tissue measured less than 10 h postmortem at frequencies from 800 to 2450 MHz. Bioelectromagnetics 24: 423–430.

Sekino M, Inoue Y, Ueno S (2004): Magnetic resonance imaging of mean values and anisotropy of electrical conductivity in the human brain. Neurol Clin Neurophysiol 30:55.

Serletis D, Bulacio J, Bingaman W, Najm I, González-Martínez J (2014): The stereotactic approach for mapping epileptic networks: A prospective study of 200 patients. J Neurosurg 121: 1239–1246.

Siemionow V, Yue GH, Barnett GH, Sahgal V, Heilbrun MP (2000): Measurement of tissue electrical impedance confirms stereotactically localized internal segment of the globus pallidus during surgery. J Neurosci Methods 15:113–117.

Shapiro S, Wilk M (1965): An analysis of variance test for normality (complete samples). Biometrika 52:591–611.

Talairach J, Bancaud J, Szikla G, Bonis A, Geier S, Vedrenne C (1974): New approach to the neurosurgery of epilepsy. Stereotaxic methodology and therapeutic results. Neurosurgery 20: 11–240.

Tidswell T, Gibson A, Bayford RH, Holder DS (2001): Three-dimensional electrical impedance tomography of human brain activity. Neuroimage 13:283–294.

Tofts PS, Branston NM (1991): The measurement of electric field, and the influence of surface charge, in magnetic stimulation. Electroencephalogr Clin Neurophysiol 81:238–239.

Van Harreveld A, Murphy T, Nobel KW (1963): Specific impedance of rabbit's cortical tissue. Am J Physiol 205:203–207.

Vorwerk J, Cho JH, Rampp S, Hamer H, Knösche TR, Wolters CH (2014): A guideline for head volume conductor modeling in EEG and MEG. Neuroimage 100:590–607.

Wolters CH, Anwander A, Tricoche X, Weinstein D, Koch MA, MacLeod RS (2006): Influence of tissue conductivity anisotropy on EEG/MEG field and return current computation in a realistic head model: A simulation and visualization study using high-resolution finite element modeling. Neuroimage 30:813–826.